Preflight Detector Characterization of BLAST-TNG

Sam Gordon[1] · **Adrian Sinclair**[1] · **Philip Mauskopf**[1,2] · **Gabriele Coppi**[3] ·
Mark Devlin[3] · **Bradley Dober**[4] · **Laura Fissel**[5] · **Nicholas Galitzki**[6] ·
Jiansong Gao[4] · **Johannes Hubmayr**[4] · **Nathan Lourie**[3] · **Ian Lowe**[3] ·
Christopher McKenney[4] · **Federico Nati**[7] · **Javier Romualdez**[3]

Abstract

The Next-Generation Balloon-borne Large-Aperture Submillimeter Telescope
(BLAST-TNG) is a submillimeter imaging polarimeter which will map the polarized
thermal emission from interstellar dust, revealing magnetic field structures in nearby
giant molecular clouds, external galaxies and the diffuse interstellar medium in three
bands centered at 250, 350 and 500-μm (spatial resolution of 30″, 41″ and 59″).
Its camera contains over 2500 dual-polarization sensitive lumped element kinetic
inductance detectors, which are read out using field-programmable gate array-based
readout electronics. BLAST-TNG was scheduled for a 28-day Antarctic flight during
the 2018/2019 summer season, but unfavorable weather conditions pushed the antic-
ipated flight to 2019/2020. We present a summary of key results from the 2018/2019
preflight characterization of the detector and receiver. Included in this summary are
detector yields, estimates of in-flight sensitivity, a measurement of the optical pass-
bands and estimates of polarization efficiency.

Keywords LEKIDs · Detector readout · Submillimeter astrophysics

✉ Sam Gordon
  sbgordo1@asu.edu

[1] School of Earth and Space Exploration, Arizona State University, Tempe, AZ 85287, USA

[2] Department of Physics, Arizona State University, Tempe, AZ 85287, USA

[3] Department of Physics and Astronomy, University of Pennsylvania, Philadelphia, PA 19104, USA

[4] National Institute of Standards and Technology, Boulder, CO 80305, USA

[5] National Radio Astronomy Observatory, Charlottesville, VA 22903, USA

[6] Department of Physics, University of California San Diego, La Jolla, CA 92093, USA

[7] Physics Department, University of Milano-Bicocca, 20126 Milan, Italy

1 Introduction

The Next-Generation Balloon-borne Large-Aperture Submillimeter Telescope (BLAST-TNG) is a submillimeter (sub-mm) imaging polarimeter which will map the polarized thermal emission from interstellar dust, revealing magnetic field structures in nearby giant molecular clouds, the diffuse interstellar medium and nearby external galaxies [1]. BLAST-TNG will observe in three 30% bands centered at 250, 350 and 500-μm (1200, 857 and 600 GHz), with diffraction-limited spatial resolution of 30″, 41″ and 59″ provided by an underfilled 2.5-m aperture primary mirror. Its sub-Kelvin receiver contains over 2500 dual-polarization sensitive horn-coupled lumped-element kinetic inductance detectors (LEKIDs) which are distributed between five readout chains: three for the 250-μm band and one each for the 350-μm and 500-μm bands. The three 250-μm readout chains correspond to three sub-arrays of a single 250-μm LEKID array. They are hereafter referred to as the 250U, 250V and 250W arrays. Each readout chain consists of a custom set of electronics based on the CASPER[1] ROACH2 field-programmable gate array (FPGA) board. The detector readout is described in [2], and other details of the design and performance of the telescope and receiver can be found in [4, 5].

BLAST-TNG was scheduled for a 28-day flight from NASA's Long-Duration Balloon Facility (LDB) near McMurdo Station, Antarctica, in winter 2018/2019. However, unfavorable weather conditions forced the flight to be rescheduled for the 2019/2020 season. This report summarizes the detector and instrumental performance as measured at NASA's Columbia Scientific Balloon Facility (CSBF), in Palestine, Texas, and at LDB, during the lead-up to the 2018/2019 flight attempt.

2 Detector and Instrumental Performance

2.1 Detector Yields

The resonant frequency of each LEKID shifts in response to absorbed optical power and fluctuations in the base temperature of the array. Depending on environmental conditions (e.g., atmospheric loading), from one observation to the next, the resonant frequencies can drift significantly in both frequency and quality factor (Q). Therefore, the process of identifying each detector's resonant frequency (channel identification) is an important aspect of LEKID detector readout. To identify each channel, the BLAST-TNG readout software performs a 'KID-finding' algorithm, which searches for resonators which satisfy Q and channel-to-channel frequency spacing thresholds. The frequency spacing threshold is 80–100 kHz. Figure 1 shows the baseline-subtracted transmission (S21) response vs. frequency for the 350-μm array after running the KID-finding software, with 626 identified resonator channels. The channels have resonant frequencies that are separated by about 1 MHz and

---

[1] https://casper.berkeley.edu/wiki/KATCP.

Table 1 Detector yields for each BLAST-TNG detector array

	250U	250V	250W	350-μm	500-μm	Total
N_{NIST}^{a}	612	612	612	775[b]	468	3079
N_{VNA}^{c}	500	521	495	683	381	2580
N_{CSBF}^{d}	390	237	412	626	326	1991
$Y_{\mathrm{VNA/NIST}}$	0.82	0.85	0.81	0.88	0.81	0.84
$Y_{\mathrm{CSBF/VNA}}$	0.78	0.45[e]	0.83	0.92	0.86	0.77

[a]Number of detectors on each array, reported by NIST

[b]Number of detectors within the readout band of 512 MHz

[c]Number of detectors identified in a May, 2018 VNA sweep

[d]Number of detectors identified in ROACH sweeps during Palestine integration

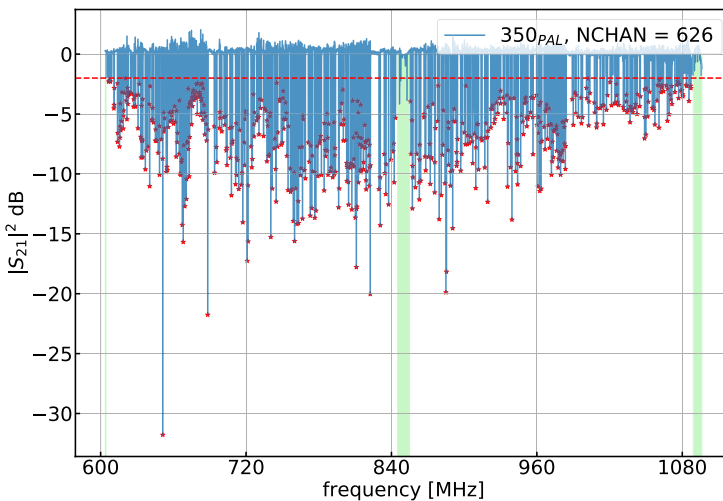[e]Low yield is the result of a malfunctioning component in the cold RF chain

Fig. 1 The output of the KID-finding algorithm, applied to a ROACH2 sweep of the 350-μm array. Red dots correspond to identified channels. The dotted red line is the dip-depth cutoff, and green bands correspond to avoidance regions. These regions are placed around the frequency of the local oscillator, which is used in the RF front ends of the readout system, or at the edges of the bands, where the gain of the system is too low due to roll-off in the system's frequency response (Color figure online)

have a width of a few kHz. The KIDs are identified by having a transmission coefficient of less than − 2 dB as shown by the dashed red line.

Table 1 lists detector yields for each readout chain (250U, 250V, 250W, 350-μm and 500-μm), measured at CSBF. As a baseline detector count, we adopt the number of channels which were found by applying the KID-finding algorithm to dark VNA sweeps of each array (N_{VNA}). These counts are compared to the number of usable

Table 2 R_P (optical responsivity) measured at NIST and NEP estimates from Palestine tests

	250-μm	350-μm	500-μm
R_P (1/pW)	1.7×10^{-5}	5.2×10^{-6}	1.6×10^{-4}
$\mathrm{NEP_{freq,Pal}}\ W/\sqrt{\mathrm{Hz}}$	35×10^{-17}	35×10^{-17}	10.0×10^{-17}

detectors on each array which were reported by NIST[2] (N_{NIST}), and to the number of usable detectors which were found at CSBF (N_{CSBF}).

The percentage yields $Y_{\mathrm{VNA/NIST}}$ and $Y_{\mathrm{CSBF/VNA}}$, shown in Table 1, are in the range of 80–85%. The low yield for the 250V array in Palestine is the result of a malfunction in the cold RF chain during the instrument integration which will be fixed prior to the 2019 flight. During the flight, the yields are expected to increase due to the higher Qs afforded by lower optical loading on the receiver.

2.2 Sensitivity

The sensitivity of each LEKID can be represented by its noise-equivalent power (NEP), in units of $W/\sqrt{\mathrm{Hz}}$. After converting the *I/Q* detector streams into a frequency shift (df) relative to their resonant frequencies, the NEP is calculated as:

$$\mathrm{NEP_{freq}} = \frac{e_f/f_0}{R_P} \quad \left[\frac{\mathrm{W}}{\sqrt{\mathrm{Hz}}}\right] \tag{1}$$

where e_f/f_0 is the fractional frequency noise in units of $1/\sqrt{\mathrm{Hz}}$ and R_P is the frequency response to optical power (optical responsivity) $(\mathrm{df}/f_0)/\mathrm{dP_{opt}}$. Average optical responsivities for each waveband, measured at NIST, are listed in Table 2, in units of 1/pW. The median NEP for each BLAST-TNG waveband was calculated during the CSBF integration, and the values are also listed in Table 2. The detector timestreams used for this calculation were taken during the optical passband measurement (see Sect. 2.3) (cryostat window exposed, looking off-source at the 300 K room).

In order to estimate the instrumental optical efficiency γ_{opt}, a differential optical measurement was performed by acquiring data with an aluminum shutter placed inside and outside of the optical path. Using the optical responsivities in Table 2, the measured frequency shift of the resonators corresponds to γ_{opt} of 10–20%. This estimate agrees with the results of previous differential measurements of the receiver which were taken using optical loads of 300 K and 77 K. The results were compared to a parametric LEKID model that takes into account the detectors' response to absorbed optical power, as well as to changes in base temperature ([3, 6]).

---

[2] The provided yield value for the 350-μm array has been decreased to account for resonators which fell outside of the 512 MHz readout bandwidth.
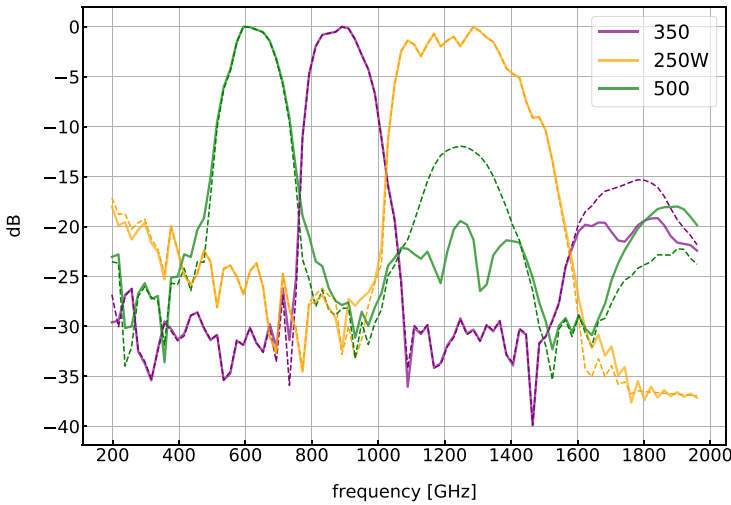
Fig. 2 BLAST-TNG optical passbands for the 250W (*orange*), 350-μm (*purple*) and 500-μm (*green*) arrays. The dashed traces are uncorrected for nonlinearity in the interferograms, and solid traces are corrected (Color figure online)

2.3 Optical Passbands

A Fourier-transform spectrometer (FTS) containing a water-cooled mercury arc lamp was used to produce in-band emission covering the three BLAST-TNG wavebands. The measurement lasted ∼ 5.5 h, during which ∼ 40 min of data was recorded for each BLAST-TNG detector with the FTS positioned in five different orientations relative to the cryostat window: centered, above-center, below-center, right-of-center and left-of-center. These positions were used to maximize the likelihood that the beam for each detector channel would be well illuminated in at least one of the positions.

Averaged interferograms for each of the five detector arrays were produced using several hundred channels containing a high signal-to-noise-ratio (SNR). Asymmetries in the interferograms due to nonlinearities in the detector response produce spurious features at multiples of the main band center. These were corrected by applying a second order polynomial to the responsivity of the detectors to correct for the reduction in responsivity when the resonator is shifted by a significant fraction of a linewidth from the probe tone.

Passband spectra for each band were produced by taking the inverse-Fourier transform of each interferogram template. The passbands for the 250W, 350-μm and 500-μm arrays are shown in Fig. 2, with their amplitudes normalized to their maximum values and expressed in dB. The solid and dashed traces show the passbands, which result from using the corrected and uncorrected interferograms, respectively.

The frequency responses of the measured passbands are far from that of ideal bandpass filters. However, the full width at half maximum (FWHM) for each band is close to the 30% design bandwidth, and adjacent channel rejection is ∼ 15 dB.
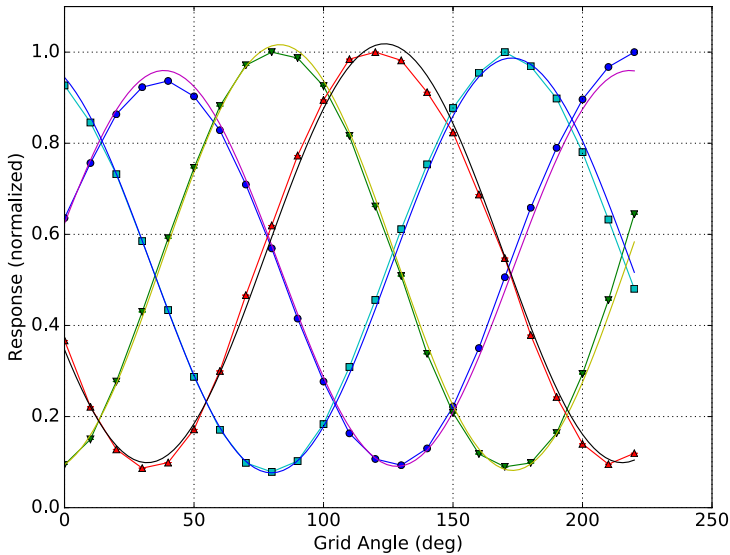
Fig. 3 Normalized polarization response for a set of four detectors in the 350-μm array. The data points correspond to the data from an individual detector in each of the four polarization angles in the array. Each pixel has two orthogonal polarization sensitive detectors, and alternating pixels have their polarization angle rotated by 45°. The statistical error bars for the individual points are slightly smaller than the size of the markers, and all of the detectors have similar response functions. Also shown are the simple models fit to the data assuming that the cross-polar efficiency and co-polar efficiency add to one. The data are normalized to have a maximum response of unity, but the models have an arbitrary amplitude and the co-polar efficiency is defined as $1 - \min_{\text{model}}/\max_{\text{model}}$ (Color figure online)

2.4 Polarization Efficiency

As a polarimeter, BLAST-TNG must be able to distinguish the signal in one linear polarization from the signal in the orthogonal polarization with high fidelity. Its ability to do so relies on having a high polarization efficiency ϵ_{pol}, or low cross-polarization efficiency ϵ_{Xpol} ($\epsilon_{\text{Xpol}} = 1 - \epsilon_{\text{pol}}$). Here, we describe the initial analysis of preflight polarization measurements.

The polarization efficiencies for the 250U, 250W and 350-μm arrays were measured at CSBF during the summer 2018 receiver integration.[3] To perform the measurements, a rotatable polarizing grid was attached to the outside of the cryostat window, and the plane of the grid was tilted 45° away from the window's plane to minimize back reflections. A chopper equipped with a heated blackbody source was placed in front of the window. The polarizing grid was then rotated by 360° in 10° intervals. At each rotation angle, detector channel timestreams were recorded with the chopper in the *on* ($T \simeq 330\,\text{K}$) and *off* ($T \simeq 300\,\text{K}$) positions. Figure 3 shows

---

[3] Data for the 250V and 500-μm arrays were not available due to excess noise during these tests. The achromatic half-wave plate (AHWP) was not installed in the receiver when these measurements were taken. Additional measurements will be required to estimate its contribution to the cross-polarization.

Table 3 Polarization efficiency for three readout chains: 250U, 250W and 350-µm

	Median $\epsilon_{\mathrm{pol}-1}$	Median $\epsilon_{\mathrm{pol}-2}$	Median $\epsilon_{\mathrm{pol}-3}$	Median $\epsilon_{\mathrm{pol}-4}$
250U-µm	0.851	0.844	–	–
250W-µm	0.831	0.834	–	–
350-µm	0.897	0.924	0.887	0.862

Whereas the 350 µm pixels have four polarization angles, the pixels of the 250 µm sub-arrays have two angles. However, the sub-arrays are arranged so that the polarization angle of the 250U pixels is rotated by 30° with respect to the 250W pixels, and by 60° with respect to the 250V pixels. The 250V detectors had excess noise due to a bad connection in the readout chain, which was repaired before flight

the normalized polarization response of four detectors which are sensitive to polarization angles separated by 45° (pol-1, pol-2, pol-3 and pol-4), as a function of 22 grid angles, for the 350-µm array. The polarization efficiencies for each of the three measured arrays are listed in Table 3. These efficiencies can be compared to the average polarization efficiency of the previous BLAST-Pol instrument of 0.8.

3 Conclusion

With its large number of LEKID detectors and large-aperture primary mirror, BLAST-TNG represents an important step in the development of LEKID-based flight instruments. We have presented estimates of detector yields, optical passbands and polarization efficiencies that indicate that BLAST-TNG is a highly capable instrument with great potential for a successful 2019/2020 flight.

References

1. N. Galitzki et al., J. Astron. Instrum. **3**, 2 (2014). https://doi.org/10.1142/S2251171714400017
2. S. Gordon et al., J. Astron. Instrum. **5**, 4 (2016). https://doi.org/10.1142/S2251171716410038
3. S. Gordon, Diss. Arizona State University (2019)
4. N. Lourie, et al., *Proceedings of SPIE 10700, Ground-based and Airborne Telescopes VII*, 1070022 (2018). https://doi.org/10.1117/12.2314380
5. N. Lourie, et al., *Proceedings of SPIE 10708, Millimeter, Submillimeter, and Far-Infrared Detectors and Instrumentation for Astronomy IX*, 107080L (2018). https://doi.org/10.1117/12.2314396
6. P.D. Mauskopf, Publ. Astron. Soc. Pacific **130**(990), 082001 (2018)